ELSEVIER

Earth and Planetary Science Letters 184 (2000) 287–303

EPSL

www.elsevier.com/locate/epsl

Topography and isotherms revisited: the influence of laterally migrating drainage divides

Kurt Stüwe [a,*], Michael Hintermüller [b]

[a] *Institut für Geologie und Paläontologie, Universität Graz, Heinrichstr. 26, A-8010 Graz, Austria*
[b] *Institut für Mathematik, Universität Graz, Heinrichstr. 36, A-8010 Graz, Austria*

Received 6 June 2000; received in revised form 16 October 2000; accepted 20 October 2000

Abstract

Drainage divides of mountain ranges will shift laterally during asymmetric erosion of the range. Such asymmetric erosion may occur due to differential precipitation on different sides of a range, or because of different topographic gradients, for example at passive margins. Here, a semi-analytical solution is presented that can be used to evaluate the shape of isotherms underneath an asymmetrically eroding, randomly shaped topography. It is shown that, because of this asymmetric erosion, cooling curves of rocks from the slowly denuding side of the range (in shift direction of divide) are characterized by a decrease in cooling rate with decreasing temperature, while cooling curves of rocks from the rapidly denuding side (in lee of the shift direction) are characterized by increasing cooling rate with decreasing temperature. Moreover, in rapidly denuding terrains, cooling through the 110°C and 75°C isotherms (approximating the retention temperatures of the apatite fission track and (U–Th)/He systems, respectively) may occur on the slowly denuding side of a range at twice the age of samples from the rapidly denuding side. In general, differences in cooling curves and cooling ages below 110°C should be recognizable in terrains where the erosion and lateral migration rates are of the order of 2 mm per year or more. In view of the recent developments of low temperature geochronological methods, our model provides an important tool to estimate the rate of lateral migration of drainage divides in regions where this is not constrained by the geomorphological record.

Keywords: topography; isotherms; low temperature; geochronology; watersheds

1. Introduction

In thermal models that are used to explain geothermometric and geochronological data collected by Earth scientists in the field, it is generally assumed that the isotherms are planar surfaces at depth. Then, it is possible to infer exhumation rates from cooling age data. Neglecting all other two- and three-dimensional effects, this assumption is valid – even for mountainous terrains – if isotherms are considered that are deep in the crust, compared with the amplitude of the topography at the surface. However, at shallower depths, isotherms will follow the topography in a damped manner. The characteristic length scale (skin depth) of this damping effect is of some relevance for the interpretation of low temperature geochronological data. For example, if erosion rates of mountain belts are estimated from

* Corresponding author. Tel.: +43-316-380-5682; Fax: +43-316-380-9870; E-mail: kurt.stuewe@kfunigraz.ac.at

0012-821X/00/$ – see front matter
PII: S0012-821X(00)00315-0

the relationship between geochronologically determined cooling ages and sample elevation [1–3], then the erosion rates will be overestimated, if the dated isotherm is shallower than this skin depth [4].

Thus, it is important to understand the curvature of isotherms at depth and a number of authors have been concerned with this subject. Earlier studies were largely concerned with the temperature distribution underneath topography in the absence of erosion [5]. These models were later expanded to account for erosion (which may enhance the effect significantly) by Stüwe et al. [4] and a time-dependent evaluation of the problem has been presented by Mancktelow and Grasemann [6]. The principal remaining limitation of these models is the assumption that the topography lowers only vertically during erosion. Field studies have shown that topography changes through time, e.g. [7–9], and that drainage divides lower not only vertically, but also shift laterally (Fig. 1); for example as the consequence of asymmetric erosion of mountain belts, e.g. [10–12]. Indeed, in many mountain belts the rates of vertical lowering and lateral shifting of the topography are comparable. For example, in the eastern European Alps in the region west of Innsbruck, the principal Alpine drainage divide appears to have shifted several tens of kilometers northwards within the last 20 myr (Fig. 1). During the same time interval, substantial parts of the eastern Alps were exhumed from depths comparable to this lateral shift (i.e. depths up to several tens of kilometers) [13]. While the shift of this drainage di-

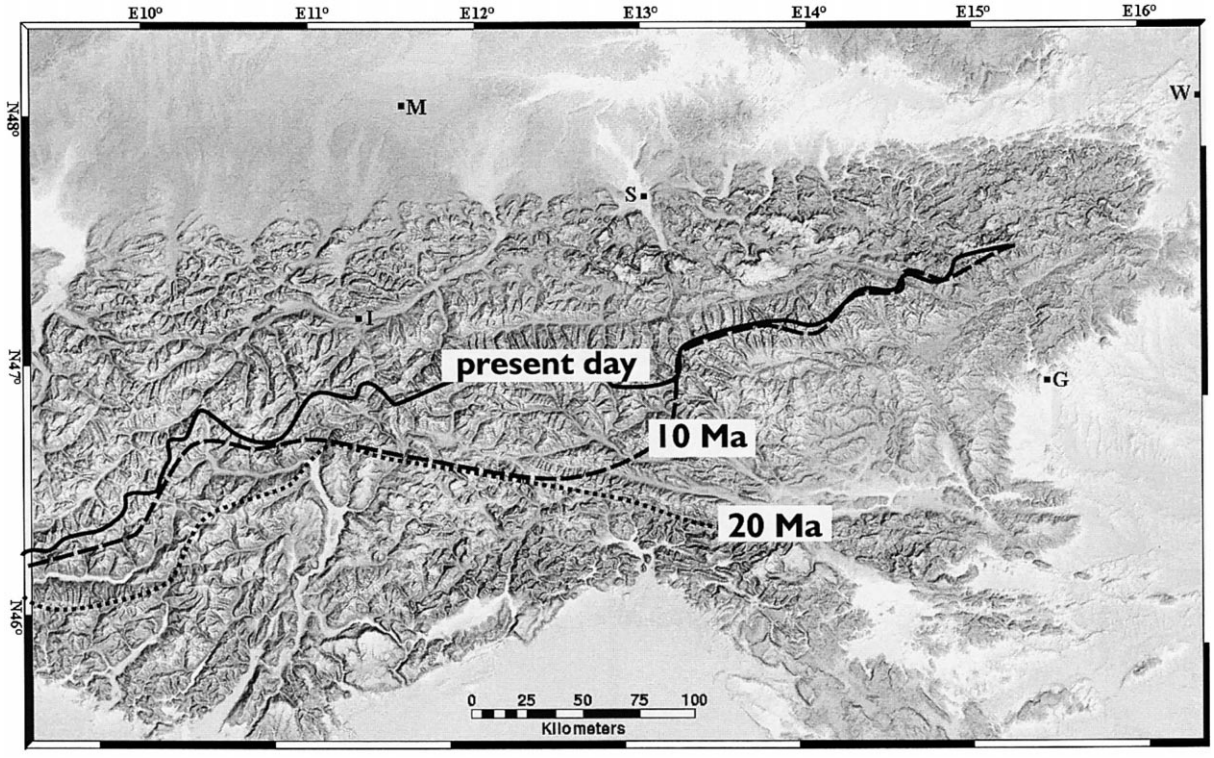

Fig. 1. Example of laterally shifting drainage divides from the eastern European Alps. The example illustrates that the rate of lateral shifts of drainage divides in mountain belts may be comparable to the rate of vertical incision of the topography. Drainage divides (thick lines) are sketched for the present day situation (solid line), 10 Ma (dashed line) and 20 Ma (dotted line) (lines by A. Kuhlemann, personal communication, 2000). The lines are sketched onto the digital elevation model of the eastern Alps (Frisch et al. [13]; Székely, personal communication, 2000) based on analyses of provenance regions of sediments in the molasse basins north and south of the Alps. Labelled cities are: G = Graz; I = Innsbruck; M = München; S = Salzburg.

vide is as yet not very well-constrained, such examples illustrate that isotherms underneath many mountain belts may be insufficiently described by thermal models which consider only vertical lowering of the topography.

In this paper we present a model that can be used to describe the thermal effects of an eroding topography that lowers vertically and migrates laterally. Our model gains particular relevance because of the rapid development of geochronological methods that can be used to date isotherms significantly below 100°C, e.g. [14–16].

1.1. Terminology

The following terminology is defined. The term steady state topography is used for a topography that stays constant in shape over time (Fig. 2). Steady state topography is called stationary when it is not being eroded and eroding if the crust is being denuded. If there are lateral changes in the vertical denudation rate, a steady state topography will shift laterally. This may be described by the constant vertical and horizontal components of a vector describing the displacement of the surface relative to the rocks. The vertical vector component is called incision rate, (here described in a Eulerian reference frame by the upwards advection rate u) and the horizontal vector component is called the migration or shift rate (here described by the lateral advection rate v) (Fig. 2). Note that our definition of incision rate does describe the vertical lowering of drainages and corresponds to the mean vertical erosion rate averaged over the whole topography. It does not describe the vertical lowering of any one vertical profile.

For the erosion of a steady state topography, u and v are the same at all points of the topography, so that drainages and drainage divides incise vertically and shift laterally at a constant rate. However, note that the denudation rate, i.e. the vertical lowering of topography at any one point of the topography, varies laterally: on Fig. 2a there is practically no vertical removal of section at location A, but substantial removal at location B. Here we will refer to the left and right sides of a range as characterized by A and B, as the dry and wet sides of a range, respectively. This is because many authors have shown that variations in vertical erosion rate, for example caused by differential precipitation in different parts of a range,

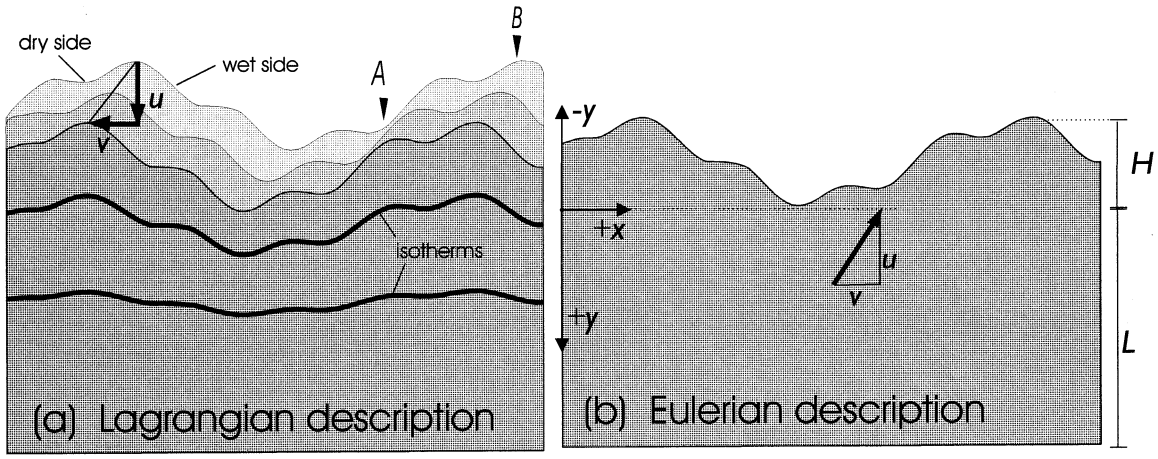

Fig. 2. Model set up, boundary conditions and choice of coordinate system. (a) In a Lagrangian reference frame, topography incises into the crust at the mean vertical rate u and lateral rate v. In a Eulerian reference frame erosion is described by upwards advection of material. Note that although u and v are constant, the rates of vertical removal of section at A and B (symbolically called 'wet' and 'dry' side of the range) are different. The topography shown is made up of the superposition of two periodic waves with the smaller wave having 1/4 of the wavelength and amplitude of the principal wavelength. This, or any other arbitrary topography may be described with the equations described in this paper.

may indeed be responsible for the shifts of drainage divides towards the dry, i.e. less-precipitation side of a range, e.g. [11,17]. However, it is emphasized that a difference in denudation rate between the different sides of a range may also be caused by different topographic gradients, for example at passive margins. Thus, our description of 'dry' and 'wet' side should be considered to be symbolic for slowly and rapidly denuding, respectively.

Furthermore we use steady state isotherm or thermal steady state to describe isotherms that do not change in shape or position with respect to the topography. Just like the topography itself, steady state isotherms do change their position in a Lagrangian reference frame as shown in Fig. 2a, but do not change in coordinates in an Eulerian reference frame which we will use here (Fig. 2b). Finally, we define exhumation and exhumation rate as the process and process rate of decreasing the vertical distance of a rock from the surface. As such we use the meaning of exhumation widely accepted in tectonics (e.g. [18,19]), but note that this is different from that used by geomorphologists, e.g. [20]. For further definitions of the terms uplift and exhumation we refer to [19].

2. The model

2.1. Previous approaches and results

Most previous accounts have simplified the problem of a periodic topography with a constant surface temperature by describing it as a problem of a periodic temperature variation along a planar surface [21–23]. This approximation is valid if the thermal gradient inside the topography is constant. For this problem, the steady state temperature variation at depth may be described by:

$$T(x,y) = T_0(y) + \Delta T \cos\left(\frac{2\pi x}{\lambda}\right) e^{ym} \qquad (1)$$

where x and y are the horizontal and vertical spatial coordinates, $T_0(y)$ describes the geotherm in the absence of any surface perturbations, λ is the wavelength of the topography, ΔT is the amplitude of the lateral temperature variation and m is given by:

$$m = \frac{1}{2}\left(-\frac{u}{\kappa} - \sqrt{\left(\frac{u}{\kappa}\right)^2 + \left(\frac{4\pi}{\lambda}\right)^2}\right) \qquad (2)$$

where u is the rate of upwards advection of material due to erosion and κ is the constant thermal diffusivity, which we always assume to be $\kappa = 10^{-6}$ m^2/s [6,23]. In essence, Eq. 1 describes a geotherm (given by $T_0(y)$) to which a perturbation by the surface temperature variation is added. It may be seen that this perturbation drops off exponentially with the characteristic length scale m. The geotherm $T_0(y)$ may be of any shape and can include heat production terms. However, for clarity, it is often assumed to be linear in the absence of erosion and is fixed by $T = T_s = 0$ at the surface and $T = T_L$ at the lower boundary at depth L, for example the base of the lithosphere. Then, the shape of the steady state geotherm during erosion at the rate u may be described by:

$$T_0(y) = T_L \cdot \left(\frac{1 - e^{-(uy/\kappa)}}{1 - e^{-(uL/\kappa)}}\right) \qquad (3)$$

This equation is equivalent to equation 8 of Stüwe et al. [4] and equation 19 of Mancktelow and Grasemann [6]. Eq. 3 has been expanded to account for radiogenic heat production by Batt and Braun [24], but in view of the uncertainties associated with our knowledge of the depth dependence of heat production we believe our estimates remain more transparent if we use Eq. 3. For no erosion, i.e. $u = 0$, a limit argument for Eq. 3 yields $T_0(y) = (T_L/L)y$, where T_L/L is the linear geothermal gradient (geotherm with no heat production), and Eq. 2 reduces to $m = -2\pi/\lambda$. Then, Eq. 1 describes the temperatures underneath lateral temperature variations (maximum variation is $2\Delta T$) on a flat surface, for example underneath land–water boundaries.

However, Eq. 1 has also been used to describe the effects of surface topography. Then, it is implicit in Eq. 1 that the origin of the vertical axis is assumed at half the elevation between valley and summits of a cosine-shaped topography and ΔT is

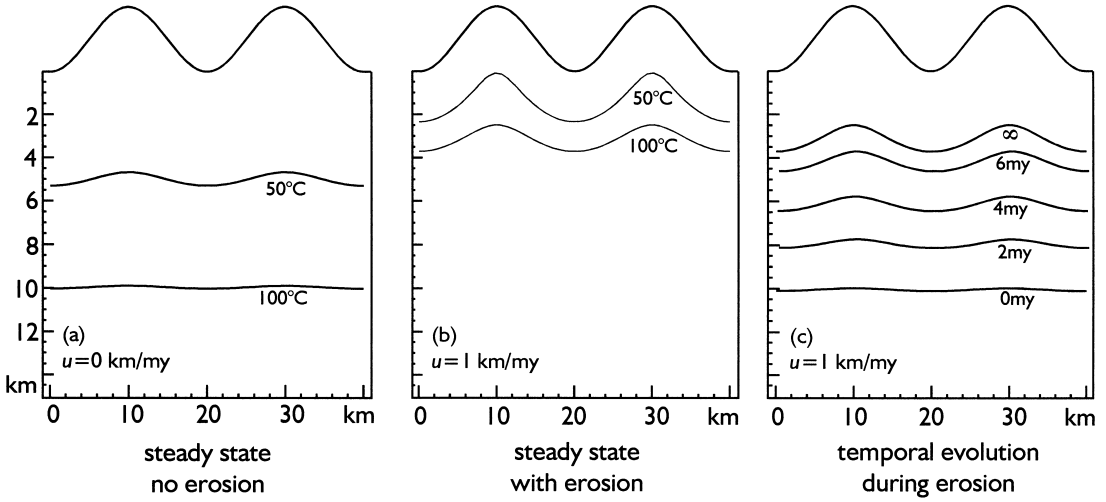

Fig. 3. Three examples of previous approaches to investigate the influence of topography on isotherms. (a) Shows the 50°C and 100°C isotherms underneath a stationary, non-eroding topography. The thermal influence of this topography was approximated with Eq. 2 assuming $u=0$ [25]. (b) Shows the 50°C and 100°C isotherms in the thermal steady state underneath a topography that incises at 1 km per year vertically into the crust [4]. (c) Shows the 100°C isotherm as a function of time (labelled in myr) in terms of its evolution from (a) to (b) [6].

given by $\Delta T=(H/2)\cdot dT/dy_{(y=0)}$, where H is the elevation of the summits of the periodic topography above the valley floors [23]. Using this solution (with $u=0$), Brown et al. [25] have shown that the interpretation of geochronologically derived apatite fission track ages will not be affected by the shape of isotherms at depth (Fig. 3a).

However, most mountainous terrains are not characterized by stationary topography, but by an eroding topography which progressively denudes the crust. The influence of this upwards advection effect of heat was considered by [4,6], assuming a steady state topography. In their approach, Stüwe et al. [4] did not use Eq. 1, but developed a model that is not limited by the assumption that the thermal gradient inside the topography is constant. Mancktelow and Grasemann [6] presented differences between Eq. 1 and the approach of Stüwe et al. [4] in their figure 11. Stüwe et al. [4] showed that – for the thermal steady state – the interpretation of apatite fission track ages may indeed be affected by surface topography, especially if the erosion rate exceeds approximately 100 m/myr for several myr (Fig. 3b). Stüwe et al. [4] also explored the influence of λ, H and u on the amplitude of the track retention isotherm at depth. Mancktelow and Grasemann [6] expanded on this problem and presented the time-dependent effects of erosion of a steady state topography (Fig. 3c).

2.2. Current approach

The principal shortcomings of the studies of Stüwe et al. [4] and Mancktelow and Grasemann [6] are that they neglect the influence of lateral gradients in the vertical erosion rate. In order to investigate this effect, we study the thermal steady state for a topography that erodes more rapidly on one side than on the other and limit our considerations to scenarios where the topography remains in the steady state so that the erosion process may be described by the constant vector components u and v (see Section 1.1 and Fig. 2). For these assumptions, an approximate analytical solution was found by following the approach of Stüwe et al. [4] and accounting for two-dimensional advection. For the coordinate system from above (with the origin of the vertical axis at the lowest point of the topography) and same boundary conditions for which Eq. 3 was derived, the dimensionless depth $Y=y/L$ of a given iso-

therm may be written as:

$$Y = Y_0 + \varepsilon\rho(Y_0,\ X) \tag{4}$$

Here $\varepsilon = H/L$, with H the maximum height of the topography, represents the topographic scale, and X is the dimensionless lateral distance $X = x/L$. Y_0 is the solution giving the temperature–depth relation in the vertically and laterally eroding case without topography. It has the form:

$$Y_0(\Theta) = -\frac{1}{\eta}\ln\left(1 + \Theta(e^{-\eta} - 1)\right) \tag{5}$$

which is equivalent to Eq. 3 expressed in terms of depth rather than temperature. The variable Θ is the dimensionless temperature $\Theta = T/T_L$ and $\eta = uL/\kappa$ is the vertical Peclet number, in which κ is the thermal diffusivity. Note that Y_0 is independent of the lateral migration rate of the topography. Due to the assumption that the height H of the topography is small compared to L, the second term in Eq. 4, $\rho(Y_0, X)$, can be interpreted as perturbation in the presence of a topography. This perturbation depends on the vertical and lateral heat advection effects. The thermal effects of lateral advection are described by the lateral Peclet number: $\mu = vL/\kappa$. The term $\rho(Y_0, X)$ is given by:

$$e^{\left(-\frac{\eta Y_0}{2}\right)}\rho(Y_0,\ X) = \alpha_0 f(X) + \sum_{n=1}^{\infty}\alpha_n \int_0^{\infty} e^{-\xi}\left(\tilde{f}^X(X + \tilde{\xi}_n) + \tilde{f}^X(X - \tilde{\xi}_n) - 2\tilde{f}^X(X)\right)d\xi \tag{6}$$

where:

$$\alpha_0 = \frac{\sinh\left(\frac{1}{2}\sqrt{\eta^2 + \mu^2}(1 - Y_0)\right)}{\sinh\left(\frac{1}{2}\sqrt{\eta^2 + \mu^2}\right)}$$

and for $n = 1, 2, \ldots$:

$$\alpha_n = (-1)^{n+1} n\pi \frac{\sin\left(n\pi(1 - Y_0)\right)}{\omega_n^2}$$

$$\omega_n = \frac{1}{2}\sqrt{4n^2\pi^2 + \eta^2 + \mu^2}$$

$$\tilde{\xi}_n = \frac{\xi}{\omega_n}$$

$f(X)$ is the normalized topography. For convenience we have also introduced $\tilde{f}^X(\tilde{X})$ which is defined by:

$$\tilde{f}^X(\tilde{X}) = e^{\left(\frac{\mu(X - \tilde{X})}{2}\right)} f(\tilde{X})$$

Note that $\tilde{f}^X(X) = f(X)$. Apart from the assumption that the topography is small in vertical extent compared to L and vanishes for large lateral distances X, no further restrictions concerning f have to be taken into account. Thus, f can be of any shape. Concerning the computation of ρ numerically we remark that the numerical evaluation of the integral in Eq. 6 is of Gauss–Laguerre type, and the infinite summation (over n) is truncated. Details on the derivation of (Y_0, ρ), and on numerical aspects are discussed in the Appendix. Also note that for no lateral migration of the topography ($\mu = 0$), the solution of [4] is recovered. In fact, the μ terms in α_0 and ω_n vanish, and $\tilde{f}^X(\tilde{X}) = f(\tilde{X})$. Thus, our approach may be viewed as a generalization of the approach of [4].

3. Model results

In order to illustrate and interpret the qualitative nature of the results, we use the model presented in Section 2.2 to evaluate isotherms, cooling curves and cooling ages initially for one set of parameters. Geologically relevant parameter ranges will then be explored in Section 3.2.

For our example, it is assumed that the lower boundary is given by the base of the lithosphere at $L = 100$ km and $T_L = 1000$°C. We also use $T_s = 0$, but note that our results for the 100°C isotherm correspond to those for the 110°C isotherm if $T_s = 10$°C. These assumptions correspond to a linear geotherm with a geothermal gradient of 10°C/km, in the absence of denudation. It is

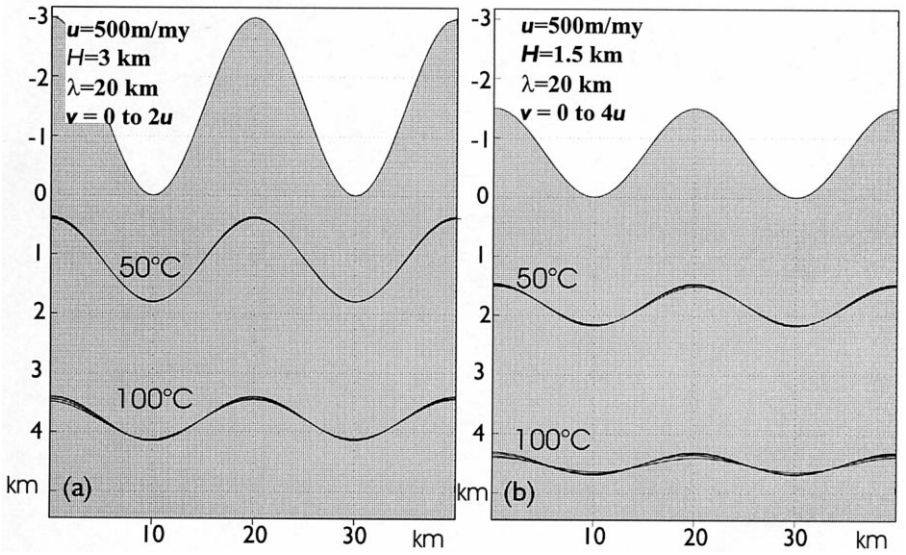

Fig. 4. Steady state isotherms underneath vertically eroding and laterally shifting topography. Amplitudes, wavelengths and erosion rates are labelled in the figure. The 50°C and 100°C isotherms are shown on both (a) and (b) for four rates of lateral shifting. Note that the shape of the isotherms with respect to the topography is largely independent of v.

emphasized that this low choice for the geothermal gradient implies that our example is conservative with respect to the amount of perturbation of isotherms and cooling paths by the surface topography. For the topography, we assume that it may be described by a periodic wave of the form:

$$h = H{\cdot}f = -\frac{H}{2}\left(1+\cos\left(\frac{2\pi x}{\lambda}\right)\right) \qquad (7)$$

Isotherms are evaluated for the central mountain of a package of nine full wavelengths of Eq. 7 centered around the middle of a grid of the width $3L$. For the topographic parameters we choose $H = 3$ km and $H = 1.5$ km and a wavelength of $\lambda = 20$ km so that the results may be directly compared with those of Stüwe et al. [4] and Mancktelow and Grasemann [6]. For the vertical advection rate we assume $u = 500$ m/myr. The rate of lateral migration of the topography v is constrained by the maximum slope of the topography. The lateral advection rate must be smaller than:

$$v = \left(\frac{\lambda}{\pi H}\right){\cdot}u \qquad (8)$$

so that peaks do not shift laterally into free air (which is mathematically possible but clearly meaningless geologically, unless differential tectonic uplift processes are invoked). At the limiting ratio of u to v given by Eq. 8 the denudation rate on the 'dry' side is zero.

Fig. 4 explores the shape and position of isotherms relative to the topography as a function of a range of lateral migration rate below the limiting value given by Eq. 8. It shows that the position of isotherms is very robust towards the magnitude of v. However, this result is somewhat misleading, as it is presented in Eulerian reference frame. Rock trajectories move diagonally through Fig. 4. This is shown on Fig. 5 where it may be seen from the crossings of particle trajectories with isotherms that cooling curves on different sides of a range will be different, depending on the ratio u/v.

In order to interpret what thermal history may be recorded in rocks that may be collected at the surface, Fig. 6 shows low temperature cooling curves of rocks during their final stages of exhumation. The 20 curves shown correspond to 10 different elevations sampled both on the 'wet' and 'dry' sides of a mountain. It may be seen

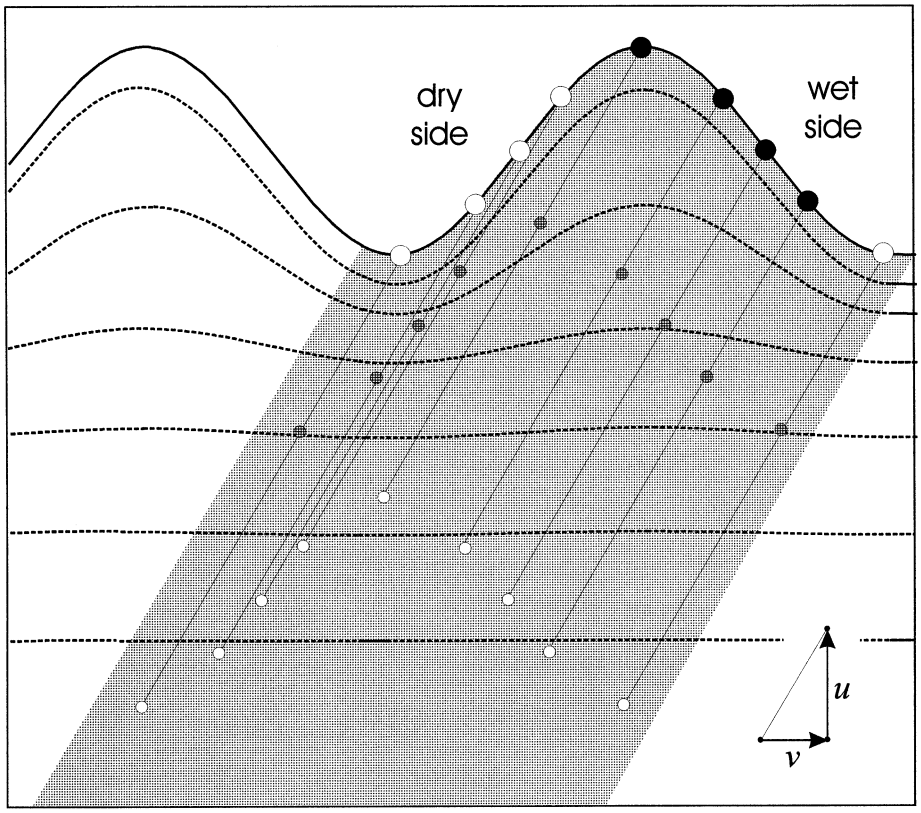

Fig. 5. Cartoon illustrating the relationship between isotherms (dashed lines) and particle trajectories (thin continuous lines). Particle trajectories (exhumation paths) are shown for rocks from five different, but constantly spaced elevations on a mountain, from both sides of the range. Positions of rocks are marked at three different times with the dots. The large dots on the surface are the samples for which cooling ages and temperature–time paths are plotted in Fig. 6 (black on high denudation side, white on low denudation side of range).

that cooling ages and temperature time paths vary significantly between the 'wet' and the 'dry' sides. Most importantly, the final cooling of rocks on the 'wet' side of a range (solid lines on Fig. 6a) is characterized by an increase in cooling rate, while final cooling to the surface on the 'dry' side of a range (dashed lines on Fig. 6a) is characterized by a decrease in cooling rate. As a consequence, rocks on the 'dry' side cool much earlier through low temperature isotherms than rocks from the 'wet' side of a mountain on the same elevation (Fig. 6b). This effect is most pronounced for intermediate elevations and it decreases or may even be reversed for higher temperature isotherms. This may be seen on Fig. 6b for the age of cooling through the 75°C and 100°C isotherms. There, samples from high elevations are older on the 'wet' side of the mountain and younger on the 'dry' side, while for samples at low elevations this relationship is reversed.

3.1. Qualitative interpretation of the model results

The result of Fig. 4 shows that the incision rate is much more important to the shape of isotherms at depth than the lateral migration rate. For high temperature isotherms this is because these are too far from the surface so that the lateral cooling through the flanks of a mountain range during sideways migration does not influence them. For low temperature isotherms this is because these are forced by the surface boundary condition to

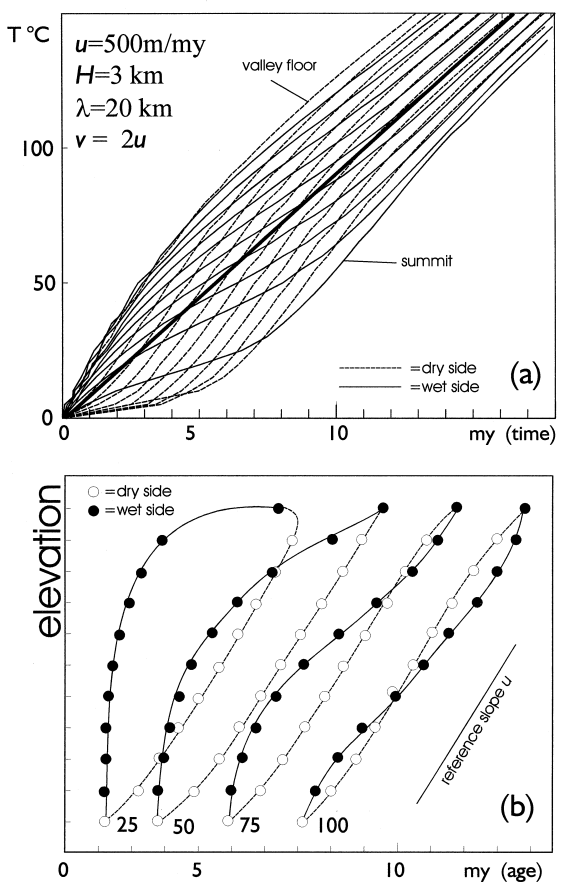

Fig. 6. Temperature–time paths and an elevation–age plot for particle trajectories of rocks now at the surface. In (a) 20 paths are shown corresponding to 10 constantly spaced elevations on the 'dry' (left side, dashed lines) and 'wet' (right side, continuous lines) sides of the mountain (see Fig. 5 for locations). The thick line marks the cooling path in the absence of topography. In (b) the time of cooling through a certain isotherm (cooling age) is shown for all rocks from (a). Black dots are for rocks from the 'dry' side of the mountain, white circles are for rocks from the 'wet' side of the mountain. Cooling ages are shown for cooling through the 25°C, 50°C, 75°C and 100°C isotherms. The small dots in (a) show the time and elevation at which the cooling ages of samples from the 'wet' and 'dry' sides of a mountain reverse.

remain inside the topography. Because of both effects, the lateral shifting of the 100°C isotherm with respect to the topography is generally less than 2% for a range of reasonable denudations rates we explored. As a consequence, lateral displacement of isotherms may generally be neglected and the simplification introduced in Section 4.2 may usually be applied instead of Eq. 4. However, it is emphasized that a constant vertical distance from the isotherm to the surface on both sides of the range does not imply that sample cooling ages on both sides are the same as the particle trajectories lie obliquely to the surface (Fig. 5).

Fig. 5 illustrates why, coming from high temperatures, cooling rates on the 'wet' side of a range must first decrease and finally increase with decreasing temperature. The initial decrease in cooling rate is because of the wider spacing of the isotherms inside the mountain; the final increase in cooling rate is because the isotherms are crossed at steeper angles at lower temperatures. Correspondingly, on the 'dry' side of the mountain, the initial increase in cooling rate is because the isotherms are narrower spaced underneath the valleys and the final decrease in cooling rate is because the final rock trajectories are near parallel to the near surface isotherms. Fig. 7 illustrates the difference between the cooling ages on the two sides of the range in some more detail using end-member scenarios for the shape of isotherms at depth. Fig. 7a shows the end-member scenario of flat isotherms. This figure corresponds to the implicit model assumptions of many interpretations of apatite fission track data [1–3]. Then, the age distribution is symmetric about the range, regardless of the ratio of vertical incision and lateral migration (i.e. the slope of the particle trajectories). Fig. 7c shows the other end-member scenario, where the isotherms are almost parallel to the surface. This figure corresponds to extremely rapid erosion rates or low temperature isotherms. Then, the age distribution is markedly asymmetric about the range with youngest cooling ages occurring in the midslope of the 'wet' side and oldest cooling ages occurring displaced from the peak towards the 'dry' side.

Note that symmetric cooling age distributions on the two different sides of a range may occur for both combinations of variables: for large lateral shift rates v combined with flat isotherms, or for low lateral shift rates and strongly perturbed

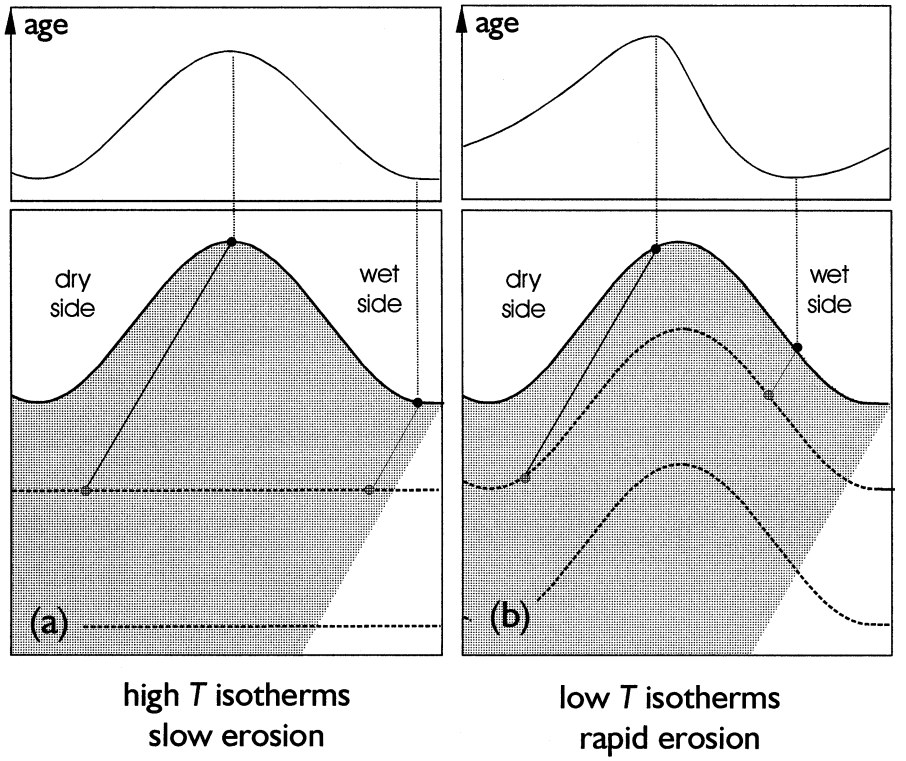

Fig. 7. Topography, isotherms, sample age for two different end-member scenarios. Particle trajectories are always drawn for the youngest and oldest sample age across the topography. In (a) isotherms are drawn parallel to the mean surface, neglecting topographic influence, as may be the case when the thermal conductivity is very high or erosion rates very slow. (b) Shows the opposite end-member scenario, where the isotherms are parallel to the surface. Note that the asymmetry of the age profile across the topography is not a function of a more rapid lateral migration rate in (b) than in (a), but is only a function of the increasing curvature of the isotherms at depth.

isotherms. On the other hand, asymmetric age distributions can only occur if the isotherms are curved and there is lateral migration of the topography. Thus, the asymmetry of the age distribution occurs because of the combination of two effects: (i) the slope of the particle trajectories with respect to the topography as given by the ratio u/v and (ii) the curvature of the isotherms as predicted by the model presented here or those by previous authors [4,6].

→

The first five columns are the elevation of the topography above the valleys (H), the distance between valleys (λ), the thermal gradient in the absence of erosion (g), the vertical incision rate u and the lateral migration rate v, respectively; as required for the implementation of Eqs. 4, 5 and 7. The sixth column lists the geothermal gradient at the surface, accounting for advection of heat, but neglecting the topography. The numbers in these columns were calculated with $dT_0/dy_{(y=0)} = T_L u/(\kappa(1-e^{(-uL/\kappa)}))$, as derived from Eq. 3. The next column gives the cooling rate at the surface, in the absence of topography, as given by the product of columns 4 and 6. In comparison with the next three columns, this value gives a good indication of the duration of cooling. For example, the cooling rate in the first row shows that the age of cooling through the 100°C isotherm is about 10 myr. The last three columns show the age difference, Δt, between two samples from the same elevation but opposite sides of the topography, sampled at the half elevation between summit and valley for three different cooling ages of 100°C, 75°C and 50°C. These numbers are positive if the samples on the dry side are older than on the wet side and negative if the sample from the wet side is older than that from the dry side. Numbers are shown in italics if they are influenced by topography outside the range considered, e.g. by a neighboring mountain. Such numbers are likely to be not very meaningful geologically.

Table 1
The influence of geologically reasonable parameter ranges on the amplitude and asymmetry of isotherms at depth

1 H (km)	2 λ (km)	3 $g = T_L$/L (°C/km)	4 u (m/myr)	5 v (m/myr)	6 $dT/dy_{(y=0)}$ (°C/km)	7 s (°C/km)	8 $\Delta t_{(100)}$ (myr)	9 $\Delta t_{(75)}$ (myr)	10 $\Delta t_{(50)}$ (myr)
1	10	10	500	1.5 u	20	10	0.0	0.0	0.2
				3.0 u			*0.0*	*0.3*	*−0.6*
			1000	1.5 u	33	33	*0.0*	0.3	0.7
				3.0 u			*0.0*	*−0.7*	0.2
		20	500	1.5 u	40	20	0.2	0.5	0.9
				3.0 u			*−0.5*	*−0.6*	1.0
			1000	1.5 u	66	66	0.7	0.8	1.0
				3.0 u			0.2	1.2	1.7
	20	10	500	3.0 u	20	10	*−0.5*	*−0.6*	0.9
				6.0 u			*−0.5*	*1.7*	*−3.0*
			1000	3.0 u	33	33	*0.0*	1.0	1.9
				6.0 u			*0.0*	*3.2*	0.6
		20	500	3.0 u	40	20	0.9	1.5	2.0
				6.0 u			*−2.5*	*−2.0*	3.0
			1000	3.0 u	66	66	1.8	2.0	1.8
				6.0 u			0.3	1.7	1.9
2	10	10	500	0.7 u	20	10	0.0	0.2	0.5
				1.5 u			0.0	0.0	0.5
			1000	0.7 u	33	33	0.4	0.5	0.6
				1.5 u			0.0	0.7	1.4
		20	500	0.7 u	40	20	0.3	0.5	0.6
				1.5 u			0.3	1.0	1.4
			1000	0.7 u	66	66	0.6	0.6	0.5
				1.5 u			1.2	1.5	1.6
	20	10	500	1.5 u	20	10	0.3	1.1	1.6
				3.0 u			*−0.8*	*−1.0*	2.0
			1000	1.5 u	33	33	1.2	1.6	1.5
				3.0 u			*−0.2*	2.1	3.5
		20	500	1.5 u	40	20	1.6	1.6	1.5
				3.0 u			1.9	3.0	3.5
			1000	1.5 u	66	66	1.5	1.4	1.1
				3.0 u			3.6	3.8	3.6
3	10	10	500	0.5 u	20	10	0.0	0.3	0.4
				1.0 u			0.0	0.2	0.7
			1000	0.5 u	33	33	0.4	0.5	0.6
				1.0 u			0.5	1.0	1.4
		20	500	0.5 u	40	20	0.4	0.5	0.6
				1.0 u			0.7	1.1	1.3
			1000	0.5 u	66	66	0.6	0.6	0.8
				1.0 u			1.4	1.5	1.6
	20	10	500	1.0 u	20	10	1.0	1.4	1.6
				2.0 u			*0.3*	1.4	2.8
			1000	1.0 u	33	33	1.4	1.4	1.4
				2.0 u			2.0	3.0	3.4
		20	500	1.0 u	40	20	1.5	1.4	1.2
				2.0 u			2.8	3.2	3.3
			1000	1.0 u	66	66	1.3	1.1	1.0
				2.0 u			3.3	3.5	3.3

(For explanation see facing page)

3.2. Quantitative influence of parameter ranges

Figs. 4 and 6 illustrate some model results using a topography with $H = 3$ km and $\lambda = 20$ km. In order to explore the influence of different topographies on isotherms at depth, Stüwe et al. [4] evaluated the amplitude of the track retention isotherm for a geologically reasonable range of H, λ and erosion rates u in their figure 6. They showed that the shape of the apatite fission track retention isotherm at depth influences the interpretation of fission track data if $u > 500$ m/myr and if $\lambda > 20$ km. At $H > 2500$ m it also has an influence for $\lambda > 10$ km and at $\lambda > 30$ km this is also true for erosion rates below $u = 500$ m/myr. Here, not only the lateral erosion rate v must be considered as an additional variable, but also the isotherms cannot be characterized by their amplitude only and their asymmetry must be characterized. Thus, it is difficult to explore and present meaningful results as a function of reasonable parameter space. Thus, we confine the interpretation of results to an evaluation of the difference in cooling age between a single sampling elevation at $h = H/2$ on different sides of a range and explore this for three characteristic 'closure temperatures' of 100°C, 75°C and 50°C (above a surface temperature of $T_s = 0$°C). These results are summarized in Table 1. There, it may be seen that cooling age differences between the different sides of a range increase with increasing amplitude and wavelength of a range and also with increasing geothermal gradient and with increasing vertical denudation rate. In particular, cooling age differences of 1–4 myr may be expected between the two different sides of a mountain for geothermal gradients above 10°C/km, λ above 10 km and erosion rates above some hundreds of meters per myr. In general, increasing the rate of lateral migration increases the difference in cooling age. In view of the absolute cooling ages (column 7 on Table 1) the differences in cooling age between the two sides of a range are of the order of 50% of the total cooling age!

However, we emphasize that cooling rates, curvature of the cooling curve and different sampling elevation may behave differently from the results summarized in Table 1, so that for a careful interpretation it will be necessary to implement our solution, for example using the simplification of Section 4.2. We suggest that the results summarized in Table 1 should not be interpreted geologically beyond the fact that they indicate that there may be significant cooling age differences between the two sides of a range due to lateral migration of the topography at geologically relevant rates.

4. Discussion

4.1. Limitations of the approach

4.1.1. The steady state assumption

Our model is derived for the thermal and topographic steady state. Thus, it is strictly only applicable to regions that have denuded long enough so that the upwards advection of heat is balanced by the cooling from the surface and there is no change of the position of the isotherms with respect to the topography over time. The model also only applies if no tectonic processes interfere with the erosional denudation process. However, this refers only to tectonic processes that perturb near surface isotherms and not to deep seated processes that will always occur in active mountain belts [24].

In order to test the influence of the thermal steady state assumption on real scenarios, Stüwe et al. [4] and also Mancktelow and Grasemann ([6], equation 60; figure 13) used an ADI finite difference time-dependent model and showed that the thermal steady state is reached extremely rapidly. Thus, our steady state solution may be used for any mountain belt that has eroded at a constant rate for more than a few 10^5 yr. The same result may be arrived at by a simple comparison of the length and time scales of equilibration using the Peclet number P_e and the thermal time constant τ. As we are considering the thermal equilibration only within the topography, we are using H as the length scale of equilibration and can define: $P_e = uH/\kappa$ and $\tau = H^2/\kappa$. For a range of realistic topographies and erosion rates, the Peclet number is always substantially smaller than 1, indicating that diffusion far out-

weighs the influence of advection in the process of shaping the isotherms at depth. Thus, τ gives a useful estimate for the time scale of equilibration of the isotherms at depth. For a range of reasonable topographies, τ is always substantially smaller than 1 myr. In summary, the model can always be applied if there was no tectonic perturbation of near surface isotherms within about 0.5 myr.

4.1.2. The assumption of periodic topography

In this paper we have evaluated the results of our model for a periodic topography. This assumption is useful to explore the influence of topography on isotherms as a function of two simple, characteristic geometric parameters: the wavelength λ and amplitude $H/2$ of the topography. However, we emphasize that the approach presented in Section 2.2 allows the description of the influence of any random topography on isotherms at depth and provides therefore a major improvement relative to the approach of [6,23]. Moreover, any random topography may be described by an appropriate summation of a series of periodic waves. Thus, it is possible to evaluate the thermal effects of a random topography, by an appropriate summation of the first few dominant wavelengths and amplitudes of a periodic topography for which results are presented in Table 1 and Fig. 5.

4.1.3. Two-dimensionality

The model presented here is two-dimensional. Thus it applies only to mountain ranges with parallel drainage patterns and infinitely long, horizontal ridges. Fortunately, many mountain belts are characterized by drainage divides that are long, compared to their width, as for example in the Southern Alps of New Zealand. However, there are examples from the Himalaya, where significant three-dimensionality of the problem has been documented [26]. Stüwe et al. [4] have suggested that the effect of three-dimensionality becomes significant enough to be considered in thermal models, if the topography at right angles to the two-dimensional cross section considered is larger than half an order of magnitude of the principal amplitude.

4.2. A model simplification

Fig. 4 shows that the shape of the isotherms relative to the topography is robust towards the rate of lateral migration of the drainage divides. Because of this, a crude first order simplification of the model presented here may be made using Eq. 1 and an appropriate variation of x and y as a function of time to describe the oblique particle trajectories relative to the topography during asymmetric erosion. When using Eq. 1 to describe cooling paths or cooling ages, the coordinates x and y must be substituted by:

$$x = x_0 + vt \tag{9}$$

and:

$$y = y_0 - ut$$

In this equation, x_0 and y_0 are the starting coordinates of a rock trajectory that is to be tracked through time. With this relationship it is straight forward to track cooling paths as far as $y = 0$. Final cooling from $y = 0$ to the surface is linear – as implicitly assumed in the boundary conditions of Eq. 1. This simplification gives a useful first order approximation of cooling paths during asymmetric erosion and is straight forward to implement, for example using MATHEMATICA.

4.3. Some potential examples

Our understanding of the lateral migration processes and rates of drainage divides in the evolution of an orogen is still in its early stages [7,10,12]. Nevertheless, there are several examples in the literature, where regional asymmetries of low temperature geochronological data have been documented using Ar/Ar and apatite fission track ages. Examples are the Olympic mountains in Washington [27], the Glarus Thrust in the Swiss Alps [28] or the Nanga Parbat region in the Himalaya [26]. However, in all of these examples, there are fundamental structures that influence the topography – cooling age relationships. In New Zealand there is a significant asymmetry of the denudation histories west and east of the

Southern Alps drainage divide, which has been been inferred to be caused by different precipitation on the different sides of the range [29–31]. However, there too, the different erosion rates are accompanied by substantial differential rock uplift rates across the Alpine thrust system and near surface isotherms are therefore tectonically perturbed. One setting where we believe our model is of relevance is the evolution of passive continental margins. While the denudation rates of such margins are extremely slow [32,33], the wavelength of passive margin ranges is very large (of the order of several hundreds of kilometers) so that isotherms will be curved, even at negligible erosion rates. Thus, according to Fig. 7, asymmetries in the geochronology may be useful to determine lateral migration rates, even at very small denudation rates. Regional imaging of the two-dimensional distribution of cooling histories in comparison with digital elevation models (for example those existing of the Australian continent [34] or the western European Alps [35]) will be useful to infer the lateral migration rates of topography caused by denudation processes alone.

5. Conclusion

In summary, we draw the following conclusions from our study:

We confirm the known fact that the shape of isotherms at depth underneath an eroding topography may be significantly perturbed by the surface topography. For erosion rates above about 1–2 mm per year, the 100°C isotherm is perturbed enough, so that its shape must be taken into account when interpreting apatite fission track results.

The shape of isotherms relative to the topography is robust with respect to the lateral migration rate of the drainage divides. However, cooling curves of rocks are significantly different on the rapidly eroding side of a laterally migrating drainage divide than they are on the slowly eroding side. On the rapidly denuding side they are characterized by an increase in cooling rate with decreasing temperature. On the slowly denuding side this relationship between cooling rate and temperature is reversed.

Cooling ages of rocks are – in general – older on the slowly denuding side of a range than they are on the rapidly denuding side. This is independent of the vertical incision rate (which may be the same on both sides of the range) and only depends on the rate of lateral migration of the drainage divide. The difference in cooling ages between the two sides of a mountain is most pronounced for low temperatures and intermediate elevations between valleys and summits. There, it may be of the order of 10% of the cooling age for the apatite fission track retention temperature, but up to 25% of the cooling age for the (U–Th)/He system.

Acknowledgements

The research group of the University of Tübingen, Germany, in particular B. Székely, A. Kuhlemann and W. Frisch, are gratefully acknowledged for providing Fig. 1 and for putting up with the stomach aches we caused them by asking to place concrete lines for drainage divides on the DEM, which may – in reality – not be all this well-constrained. R. Brown, D. Fabel, N. Mancktelow and M. Rahn are thanked for a series of discussions of the problem discussed here and K. Kunisch for his continued interest and support of this project. M. Summerfield, K. Gallagher and M. Sandiford are thanked for their thoughtful and helpful reviews. K.S. acknowledges the support for this project by FWF project P-12846-GEO.*[AH]*

Appendix

Let $T = T(x, y, t)$ be the temperature distribution in a homogeneous isotropic solid, with x describing the lateral distance, y the depth (positive downwards from the lowest point of a topography), and t the time. In the presence of a vertical

(in the upward direction) and a lateral material velocity, i.e. the vertical and lateral rates of displacement of the surface with respect to the rocks u and v, respectively, T satisfies the following two-dimensional partial differential equation:

$$\left.\begin{aligned} &\frac{\partial T}{\partial t}=\kappa\left(\frac{\partial^2 T}{\partial x^2}+\frac{\partial^2 T}{\partial y^2}\right)+u\frac{\partial T}{\partial y}+v\frac{\partial T}{\partial x}\\ &T(x,\ F(x),\ t)=0,\ T(x,\ L,\ t)=T_L,\\ &\quad T(x,\ y,\ 0)=\frac{T_L}{L}y \end{aligned}\right\} \qquad (10)$$

where κ is the thermal diffusivity independent of the temperature and constant in (x, y), and $F(x)$ is a given topography. Note that due to our vertical reference frame $F(x)$ is always negative. Moreover, L denotes a large depth with T_L as corresponding fixed temperature.

Transition from Eq. 10 to its dimensionless counterpart is achieved by introducing the new variables:

$$X=\frac{x}{L},\ \Theta=\frac{T}{T_L},\ \tau=\frac{\kappa t}{L^2},\ Y=\frac{y}{L}$$

In addition, let $f(X)$ be the normalized topography, and $\varepsilon=H/L$ the topographical scale.

Since we are interested in isotherms, we focus on the isothermal formulation of the dimensionless form of Eq. 10. In the resulting (non-linear) partial differential equation below we denote by subscripts partial differentiation with respect to the specified variable(s):

$$\left.\begin{aligned} &Y_\tau=Y_{XX}+Y_{\Theta\Theta}\left(\frac{1+Y_X^2}{Y_\Theta^2}\right)\\ &\quad -Y_X\left(\frac{2Y_{X\Theta}}{Y_\Theta}+\mu\right)-\eta\\ &Y(X,\ 0,\ \tau)=\varepsilon f(X),\ Y(X,\ 1,\ \tau)=1,\\ &\quad Y(X,\ \Theta,\ 0)=T_L Y \end{aligned}\right\} \qquad (11)$$

where $\mu=vL/\kappa$ and $\eta=uL/\kappa$ are the (dimensionless) lateral and vertical displacement rates of the surface with respect to the rocks, respectively.

In the present study we restrict ourselves to the steady state situation, i.e. $Y_\tau=0$. Then, in the case without topography, i.e. $\varepsilon=0$, the solution of Eq. 11 is given by:

$$Y_0(\Theta)=-\frac{1}{\eta}\ln\left(1+\Theta(e^{-\eta}-1)\right)$$

Note that Y_0 is independent of μ. Due to the assumption that the topographical height H is small compared to the depth L, ε is small. Thus, the general solution of Eq. 11 has the form:

$$Y=Y_0+\varepsilon\rho(Y_0,\ X)$$

Using this expression in Eq. 11 and neglecting terms of order ε^2 or higher, we arrive at:

$$\left.\begin{aligned} &\rho_{XX}+\rho_{Y_0Y_0}-\mu\rho_X-\eta\rho_{Y_0}=0\\ &\rho(0,\ X)=f(X),\ \rho(1,\ X)=0 \end{aligned}\right\} \qquad (12)$$

Next we apply the simple transformation:

$$\rho(Y_0,\ X)=e^{\left(\frac{\mu X+\eta Y_0}{2}\right)}\bar{\rho}(Y_0,\ X)$$

to eliminate the first order terms in Eq. 12. We obtain:

$$\left.\begin{aligned} &\bar{\rho}_{Y_0Y_0}+\bar{\rho}_{XX}-\tfrac{1}{4}(\mu^2+\eta^2)\bar{\rho}=0\\ &\bar{\rho}(0,\ X)=e^{\left(-\frac{\mu X}{2}\right)}f(X)=:\bar{f}(X),\ \bar{\rho}(1,\ X)=0 \end{aligned}\right\} \qquad (13)$$

Applying the Fourier transform $\hat{\rho}(Y_0,\ k)=\int_{-\infty}^{\infty}\bar{\rho}(Y_0,\ X)e^{-ikX}dX$ to Eq. 13, solving the resulting ordinary differential equation for ρ, and inverting the Fourier transform yields:

$$\bar{\rho}(Y_0,\ X)=\alpha_0\bar{f}(X)+\sum_{n=1}^{\infty}\alpha_n$$

$$\int_0^{\infty}e^{-\xi}\left(\bar{f}\left(X+\frac{\xi}{\omega_n}\right)+\bar{f}\left(X-\frac{\xi}{\omega_n}\right)-2\bar{f}(X)\right)d\xi$$

with α_i, $i=0, 1, 2,\ldots$, as specified in the text. Inverting the second transformation results in the solution given in Eqs. 4–6. The numerical realiza-

tion of the integrals with infinite upper limit is based on a Gauss–Laguerrian quadrature utilizing the first 15 Laguerre polynomials. Details concerning the computation of weights and nodes can be found in [36] or [37]. Moreover, the infinite summation is truncated at $n = 100$ since increasing n beyond 100 yields no significant change in the approximation.

References

[1] A.J.W. Gleadow, P.G. Fitzgerald, Uplift history of the Transantarctic mountains: new evidence from fission track dating of basement apatite in the Dry Valleys area, southern Victoria Land, Earth Planet. Sci. Lett. 82 (1987) 1–14.

[2] P.G. Fitzgerald, A.J.W. Gleadow, Fission track geochronology, tectonics and structure of the Transantarctic mountains in northern Victoria Land, Antarctica, Chem. Geol. 73 (1988) 169–198.

[3] P.A. Armstrong, T.A. Ehlers, P.J.J. Kamp, K.A. Farley, D.S. Chapman, Tracking changes in exhumation rates using low-temperature thermochronometry: an example from the Wasatch mountains, Utah (USA), in: W.P. Noble, P.B. O'Sullivan, R.W. Brown (Eds.), 9th International conference on fission track dating and thermochronology, Geol. Soc. Austral. Abstr. Vol. 58, Lorne, 2000, pp. 355–356.

[4] K. Stüwe, L. White, R. Brown, The influence of eroding topography on steady state isotherms. Application to fission track analysis, Earth Planet. Sci. Lett. 124 (1994) 63–74.

[5] S.V. Roberts, D.W. Burbank, Uplift and thermal history of the Teton Range (northwestern Wyoming) defined by apatite fission track dating, Earth Planet. Sci. Lett. 118 (1993) 295–309.

[6] N.S. Mancktelow, B. Grasemann, Time-dependent effects of heat advection and topography on cooling histories during erosion, Tectonophysics 270 (1997) 167–195.

[7] W. Frisch, J. Kuhlemann, I. Dunkl, A. Brügl, Palinspastic reconstruction and topographic evolution of the Eastern Alps during late Tertiary tectonic extrusion, Tectonophysics 297 (1998) 1–15.

[8] J. Kuhlemann, Evidence from sediment budget calculations for Miocene large scale shifts of the drainage divide in the Swiss and western Alps, in: B. Székely, W. Frisch, J. Kuhlemann, I. Dunkl (Eds.), 4th Workshop on alpine geological studies, Tübinger geowiss. Arb. Series A 52, 1999, pp. 163–165.

[9] A. Brügel, Provenances of alluvial conglomerates from the eastalpine foreland: Oligo-/Miocene denudation history and drainage evolution of the eastern Alps, Tübinger geowiss. Arb. 40, 1998, 168 pp.

[10] K. Stüwe, Flexural constraints on the denudation of asymmetric mountain belts, J. Geophys. Res. 96 (1991) 10401–10408.

[11] M.S. Steckler, G.I. Omar, Controls on the erosional retreat of the uplifted flanks at the Gulf of Suez and northern Red Sea, J. Geophys. Res. 99 (1994) 12159–12174.

[12] S.D. Willet, Orogeny and orography: The effects of erosion on the structure of mountain belts, J. Geophys. Res. 104 (1999) 28957–28981.

[13] W. Frisch, B. Székely, J. Kuhlemann, I. Dunkl, Geomorphological evolution of the Eastern Alps in response to Miocene tectonics, Z. Geomorph. 44 (2000) 103–138.

[14] M.A. House, B.P. Wernicke, K.A. Farley, Dating topography of the Sierra Nevada, California, using apatite (U–Th)/He ages, Nature 396 (1998) 66–69.

[15] A. Fleming, M.A. Summerfield, J.O. Stone, L.K. Fifield, R.G. Cresswell, Denudation rates for the southern Drakensberg escarpment, SE Africa, derived from in situ produced cosmogenic 36Cl: initial results, J. Geol. Soc. Lond. 156 (1999) 209–212.

[16] P.K. Zeitler, U–Th/He dating rides again, in: W.P. Noble, P.B. O'Sullivan, R.W. Brown (Eds.), 9th International conference on fission track dating and thermochronology, Geol. Soc. Austral. Abstr. Vol. 58, Lorne, 2000, pp. 355–356.

[17] H. Kooi, C. Beaumont, Escarpment evolution on high-elevation rifted margins: Insights derived from a surface processes model that combines diffusion, advection and reaction, J. Geophys. Res. 99 (1994) 12191–12209.

[18] P.C. England, P. Molnar, Surface uplift, uplift of rocks and exhumation of rocks, Geology 18 (1990) 1173–1177.

[19] K. Stüwe, T.D. Barr, On uplift and exhumation during convergence, Tectonics 17 (1998) 80–88.

[20] R.L. Bates, J.A. Jackson, Glossary of Geology, 3rd edn., Am. Geol. Inst., VA, 1987, 788 pp.

[21] F. Birch, Flow of heat in the front range, Colorado, Bull. Geol. Soc. Am. 61 (1950) 567–630.

[22] H.S. Carslaw, C.J. Jaeger, Conduction of Heat in Solids, Clarendon, Oxford, 1959, 510 pp.

[23] D.L. Turcotte, G. Schubert, Geodynamics. Application of Continuum Physics to Geological Problems, Wiley, New York, 1982, 450 pp.

[24] G.E. Batt, J. Braun, On the thermomechanical evolution of compressional orogens, Geophys. J. Int. 128 (1997) 364–382.

[25] R.W. Brown, Backstacking apatite fission track stratigraphy: A method for resolving the erosional and isostatic rebound components of tectonic uplift histories, Geology 19 (1991) 74–77.

[26] D.A. Schneider, M.A. Edwards, W.S.F. Kidd, A.A. Kahn, L. Seeber, P.K. Zeitler, Tectonics of Nange Parbat, western Himalaya: synkinematic plutonism within the doubly vergent shear zones of a crustal-scale pop-up structure, Geology 27 (1999) 999–1002.

[27] M.T. Brandon, M.K. Roden-Tice, G.I. Garver, Late Cenozoic exhumation of the Cascadia accretionary wedge in the Olympic mountains, northwest Washington State, Geol. Soc. Am. Bull. 110 (1998) 985–1009.

[28] M.K. Rahn, B. Grasemann, Fission track and numerical thermal modeling of differential exhumation of the Glarus thrust plane (Switzerland), Earth Planet. Sci. Lett. 169 (1999) 245–259.
[29] P.J.J. Kamp, P.F. Green, S.H. White, Fission track analysis reveals character of collisional tectonics in New Zealand, Tectonics 8 (1989) 169–195.
[30] P.J.J. Kamp, J.M. Tippett, Dynamics of Pacific plate crust in the south island (New Zealand) zone of oblique continent–continent convergence, J. Geophys. Res. 98 (1993) 16105–16118.
[31] G.E. Batt, J. Braun, The tectonic evolution of the Southern Alps, New Zealand: insights from fully thermally coupled dynamical modelling, Geophys. J. Int. 136 (1999) 403–420.
[32] H.A.P. Cockburn, R.W. Brown, M.A. Summerfield, M.A. Seidl, Quantifying passive margin denudation and landscape development using a combined fission-track thermochronology and cosmogenic isotope analysis approach, Earth Planet. Sci. Lett. 179 (2000) 429–435.
[33] K. Gallagher, R. Brown, Denudation and uplift at passive margins: the record on the Atlantic margin of southern Africa, Phil. Trans. R. Soc. Lond. 357 (1999) 835–859.
[34] A.J.W. Gleadow, B.P. Kohn, P.B. O'Sullivan, R.W. Brown, K. Gallagher, Fission track thermotectonic and denudation imaging of the Australian continent, in: W.P. Noble, P.B. O'Sullivan, R.W. Brown (Eds.), 9th International conference on fission track dating and thermochronology, Geol. Soc. Austral. Abstr. Vol. 58, Lorne, 2000, pp. 131–132.
[35] M.K. Rahn, D. Seward, A revised study of the exhumation of the central Alps: first results from a compilation of more than 500 published and new apatite fission track analyses, in: W.P. Noble, P.B. O'Sullivan, R.W. Brown (Eds.), 9th International conference on fission track dating and thermochronology, Geol. Soc. Austral. Abstr. Vol. 58, Lorne, 2000, pp. 275–276.
[36] J. Stoer, R. Bulirsch, Introduction to Numerical Analysis, Springer-Verlag, New York, 1993, 660 pp.
[37] A.H. Stroud, Numerical Quadrature and Solution of Ordinary Differential Equations, Springer-Verlag, New York, 1974, 338 pp.